2-11-2019

Misaligned Accretion Disc Formation via Kozai-Lidov Oscillations

Alessia Franchini
University of Nevada, Las Vegas, alessia.franchini@unlv.edu

Rebecca G. Martin
University of Nevada, Las Vegas, rebecca.martin@unlv.edu

Stephen H. Lubow
Space Telescope Science Institute

Monthly Notices of the ROYAL ASTRONOMICAL SOCIETY

MNRAS **485,** 315–325 (2019) doi:10.1093/mnras/stz424
Advance Access publication 2019 February 11

Misaligned accretion disc formation via Kozai–Lidov oscillations

Alessia Franchini [1]★ Rebecca G. Martin[1] and Stephen H. Lubow [2]

[1]*Department of Physics and Astronomy, University of Nevada, 4505 South Maryland Parkway, Las Vegas, NV 89154, USA*
[2]*Space Telescope Science Institute, 3700 San Martin Drive, Baltimore, MD 21218, USA*

Accepted 2019 February 7. Received 2019 February 7; in original form 2018 December 27

ABSTRACT

We investigate the formation and evolution of misaligned accretion discs around the secondary component of a binary through mass transfer driven by Kozai–Lidov (KL) oscillations of the circumprimary disc's eccentricity and inclination. We perform smoothed particle hydrodynamics simulations to study the amount of mass transferred to the secondary star as a function of both the disc and binary parameters. For the range of parameters we explore, we find that increasing the disc aspect ratio, viscosity parameter, and initial inclination as well as decreasing the binary mass ratio leads to larger amount of mass transfer, up to a maximum of about 10 % of the initial mass of the primary disc. The circumsecondary disc forms with a high eccentricity and a high inclination and is also able to undergo KL oscillations. The circumsecondary disc oscillations have a shorter period than those in the disc around the primary. We find that some of the material that escapes the Roche lobe of the two components forms a misaligned circumbinary accretion disc. This study has implications for disc evolution in young binary star systems.

Key words: accretion, accretion discs – hydrodynamics – planets and satellites: formation – binaries: general.

1 INTRODUCTION

The recent improvements in observational technology have enabled the discovery of thousands of exoplanets over the last 30 years. Roughly 40–50 % of them are expected to be hosted in binary star systems (Horch et al. 2014). It is therefore important to understand planet formation and evolution in binary systems in order to be able to explain exoplanet properties. Furthermore, it is crucial to study the birthplace of planets, the protoplanetary discs, to answer many questions about exoplanetary systems.

In a young binary star system, the accretion disc around each star may be misaligned with respect to the plane of the binary. There are a few observed misalignments in wide binary systems with separations greater than 40 au (Jensen et al. 2004; Roccatagliata et al. 2011). *HST* and recent ALMA observations showed a misalignment between the two accretion discs in the young system HK Tau (Stapelfeldt et al. 1998; Jensen & Akeson 2014). This suggests that during the formation process these systems might be subjected to small-scale perturbations, such as turbulence (Bate, Lodato & Pringle 2010; Offner et al. 2010; Bate 2012), that can result in the misalignment between the gas orbiting the two components of the binary. Numerical simulations have also shown that accretion of material on to forming stars occurs in different directions overtime. Therefore, misaligned accretion discs are likely to be typical rather than rare cases (Bate 2009, 2012, 2018).

To date, hundreds of planets have been also observed to lie in eccentric orbits with eccentricities up to about 0.9 (Tamuz et al. 2008; Moutou 2009; O'Toole et al. 2009). A planet embedded in a gaseous disc will undergo damping of eccentricity and inclination (Xiang-Gruess & Papaloizou 2013) unless it is subject to planet–planet scattering or secular perturbations (Ford & Rasio 2008; Lubow & Martin 2016). In this paper, we investigate the effects of secular perturbations, specifically the Kozai–Lidov (KL) mechanism (Kozai 1962; Lidov 1962). This is a secular effect that likely explains the eccentricities and inclinations observed in exoplanets (Wu & Murray 2003). This process periodically exchanges the eccentricity with the inclination of a misaligned test particle around one component of a binary system, if its initial inclination is above a certain critical angle.

For the first time, Martin et al. (2014) found that the KL mechanism can operate also in a fluid accretion disc. The disc remains relatively flat, i.e. not strongly warped, and the eccentricity is roughly constant in radius. The disc then responds in a global fashion to the KL oscillations. Fu, Lubow & Martin (2015a) explored further the parameter space and found that the oscillations occur over a fairly broad range of disc and binary parameters. The oscillations are damped on a time-scale of a few tens of binary orbits due to the effect of the disc viscosity (e.g. King et al. 2013). The alignment time-scale may be longer than the lifetime of the disc, meaning that some discs are likely to be dispersed before they have

★ E-mail: alessia.franchini@unlv.edu

a chance to align with the orbital plane. If a planet remains at or below the critical KL angle after the disc has been dispersed, the planet will remain stable against KL oscillations (Lubow & Martin 2016; Martin et al. 2016). Disc self-gravity can suppress KL disc oscillations (Batygin 2012; Fu, Lubow & Martin 2015b, 2017). Self-gravity likely plays an important role during the earliest phases of star formation, prior to the T Tauri phase (Kratter & Lodato 2016). As the disc accretes without being resupplied by infalling gas, its level of self-gravity is reduced and KL oscillations can commence. We report here on the evolution of a misaligned disc at this stage, idealized by neglecting the disc self-gravity.

In this paper, we explore for the first time a process by which circumprimary disc material is transferred to a secondary star that does not initially have a disc. We consider an initially highly misaligned circular circumprimary disc. The disc undergoes an increase of its radial extent due to the substantial eccentricity it acquires during KL oscillations. If this circumprimary disc extends beyond the Roche lobe of the primary star, it can then transfer mass to the companion star. This Roche lobe overflow can lead to the formation of an accretion disc around the secondary star. The investigation of the mass transfer mechanism is important for understanding the evolution of misaligned accretion discs in binaries. Furthermore, this process may affect the conditions for planet formation.

The outline of the paper is as follows. In Section 2, we consider inclined test particle orbits around one component of binary as a guide to some properties of a disc. In Section 3, we present the results of smoothed particle hydrodynamics (SPH) simulations for the formation of the circumsecondary disc by mass transfer from the primary disc that is undergoing KL oscillations. In Section 4, we discuss the formation of a circumbinary disc as a result of the KL oscillations of the circumprimary disc (and possibly the circumsecondary disc). Finally, we draw our conclusions in Section 5.

2 TEST PARTICLE ORBITS

We consider inclined test particle orbits around one component of a circular orbit binary with semimajor axis a. An initially circular test particle orbit undergoes KL oscillations if the initial inclination $i_{\rm p0}$ is in the range

$$\cos^2 i_{\rm p0} \; < \; \cos^2 i_{\rm cr} = 3/5\,, \tag{1}$$

which corresponds to the inclination range $39^\circ \leq i_{\rm p0} \leq 141^\circ$ (Kozai 1962; Lidov 1962). From this condition, it follows that there is an upper limit on the eccentricity that can be achieved during these oscillations (Innanen et al. 1997). Overlong time-scales, a particle's orbital energy, and therefore its semimajor axis $a_{\rm p}$ are conserved because the secular potential is static. In addition, the component of the angular momentum perpendicular to the binary orbital plane is conserved. These two conditions imply

$$\sqrt{1-e_{\rm p}^2}\,\cos i_{\rm p} \approx {\rm const}\,, \tag{2}$$

where $e_{\rm p}$ and $i_{\rm p}$ are the eccentricity and the inclination of a test particle orbiting one of the binary stars. The eccentricity of the particle increases from $e = 0$ up to

$$e_{\rm max} = \sqrt{1-\frac{5}{3}\cos^2 i_{\rm p0}}\,, \tag{3}$$

while its inclination decreases from $i_{\rm p0}$ to $i_{\rm cr}$.

Test particle orbits provide some indication of the behaviour of fluid discs undergoing KL oscillations in hydrodynamical simulations (Martin et al. 2014). The disc KL eccentricity approximately agrees that of particles. However, dissipation limits the disc eccentricity, especially at high eccentricity. Particle orbits also provide an estimate of the disc tilt oscillation frequency when suitably averaged in radius. The misaligned circumprimary disc is assumed to be initially circular and therefore its eccentricity oscillates from 0 to roughly $e_{\rm max}$ for a particle given by equation (3), provided that $e_{\rm max}$ is mild.

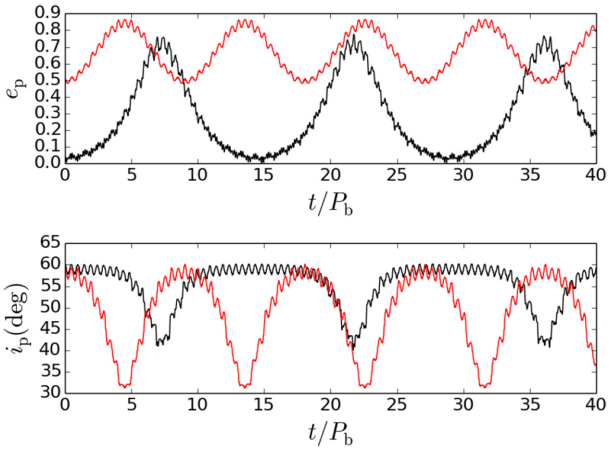

Figure 1. Eccentricity and inclination evolution of a test particle around one of the component of an equal mass circular orbit binary. The particle is initially at apastron at distance of $d = 0.2\,a$ from the secondary component. The black line refers to an initially circular particle orbit, $e_{\rm p0} = 0$, while the red line represents the case with initial non-zero eccentricity, $e_{\rm p0} = 0.5$ and initial argument of periapsis $\omega_0 = 0^\circ$.

As we will see in the next section, the circumsecondary disc that forms through mass transfer has an initial non-zero eccentricity. In order to understand the disc properties, we need to take into account the initial non-zero eccentricity of the disc. To obtain an estimate of the KL oscillation period in case of an initially eccentric accretion disc, we can carry out test particle calculations.

We consider an equal mass binary and so either star could be regarded as primary. Since we are interested in circumsecondary disc formation, we regard the particle to be orbiting the secondary star. We define a reference direction to be along a line from the primary star to the secondary star at the initial time. We determine particle orbits that start with inclination $i_0 = 60^\circ$, longitude of ascending node 0°, true anomaly of 180° (apastron), distance from secondary $d = 0.2a$, and argument of periapsis $\omega_0 = 0^\circ$. Fig. 1 shows the eccentricity and inclination evolution for such a test particle on an initially circular ($e_{\rm p0} = 0$) orbit and initially eccentric ($e_{\rm p0} = 0.5$) orbit.

Comparing the black (initially circular) and red (initially eccentric) curves in Fig. 1, we see that the period of the KL oscillations for the initially eccentric orbit case is shorter than the initially circular case by roughly a factor 2, for same initial apastron radius. The KL oscillation period depends on tidal torques that vary with radius.

We have verified that the results are insensitive to the initial value of the longitude of the ascending node, as is expected by secular theory (Fabrycky & Tremaine 2007). We also find that the KL oscillation periods for initially eccentric particle orbits for $e_{\rm p0} = 0.5$ are shorter for other initial angles of periapsis, $\omega_0 = 90^\circ$, 180°, and 270°, with initial distance $d = 0.2a$ at apastron.

Another effect associated with starting at non-zero particle eccentricity is that the minimum tilt angle $i_{\rm min}$ generally differs from the $i_{\rm cr} = 39.2^\circ$ value for the initially circular orbit case, as

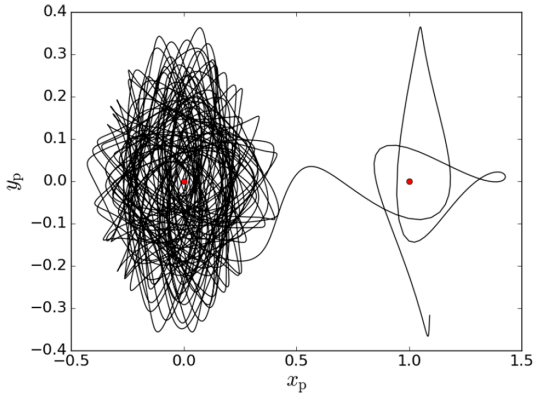

Figure 2. Test particle trajectory in the x_p−z_p plane that begins around the primary star at distance $0.36\,a$ from the star with initial tilt of $i_{p0} = 60^\circ$. The particle gains eccentricity and eventually is transferred to the secondary star. The particle trajectory is identified by the black lines and the binary component by the two red dots.

seen in Fig. 1. As seen in upper panel of fig. 2 in Fabrycky & Tremaine (2007), i_{min} is less than i_{cr} for $45^\circ > \omega_0 > 0$ and i_{min} is greater than i_{cr} for $90^\circ > \omega_0 > 45^\circ$.

In Section 3, we show through SPH simulations that the circumsecondary disc forms with non-zero eccentricity and undergoes KL oscillations with a period that is shorter by roughly a factor 2 with respect to the KL period of the (initially circular) circumprimary disc, in agreement with our test particle calculations.

3 CIRCUMSECONDARY DISC FORMATION

We show here that a misaligned accretion disc around a primary star that undergoes KL oscillations of eccentricity and inclination can become eccentric enough to overflow its Roche lobe and transfer mass on to the secondary companion. We define a Cartesian coordinate system (x_p, y_p, z_p) that is centred on the primary and corotates with the binary. The x_p-axis is along the line that joins the two stars. The z_p-axis is parallel to the binary angular momentum. Fig. 2 plots a trajectory of a test particle in the x_p−z_p plane that begins orbiting the primary star. The particle starts along the line joining the two stars at distance $0.36\,a$ from the primary on a circular orbit around the primary that is tilted by $i_{p0} = 60^\circ$ from the binary orbital plane. The particle undergoes KL oscillations and reaches a large enough eccentricity to be transferred to the secondary star through Roche lobe overflow. The particle is transferred when it is near apastron and at the part of its orbit that has the highest distance above the binary orbital plane.

To study the behaviour of discs, we perform SPH numerical simulations using the code PHANTOM (Lodato & Price 2010; Price & Federrath 2010; Price 2012; Price et al. 2017). Misaligned discs in binary systems have been extensively studied with PHANTOM (e.g. Nixon 2012; Nixon, King & Price 2013; Doğan et al. 2015; Nixon & Lubow 2015). We perform SPH simulations using $N = 5 \times 10^5$ particles. The resolution of the simulation depends on N, the viscosity parameter α, and the disc scale height H. The Shakura & Sunyaev (1973) viscosity parameter is modelled by adapting artificial viscosity according to the approach of Lodato & Price (2010). The main implication of this treatment is that in order to provide a constant α in the disc, the disc scale height H must be uniformly resolved. This is achieved by choosing both a surface density profile and a temperature profile that ensures this condition (Lodato & Pringle 2007), as discussed next.

Disc evolution strongly depends on the value of the protoplanetary discs viscosity, which is not well known. In our simulations, we model disc viscosity using the artificial viscosity parameter α_{AV} (Lodato & Price 2010). The main consequence of modelling the disc viscosity through the artificial viscosity parameter is that there is a lower limit below which a physical viscosity is not resolved in SPH ($\alpha_{AV} \approx 0.1$). Viscosities smaller than this value can produce disc spreading that is independent of the value of α_{AV} (Bate, Bonnell & Price 1995; Meru & Bate 2012).

Previous simulations of discs undergoing KL oscillations were performed with a locally isothermal temperature profile centred on the primary star. Since we are interested in disc formation around the secondary, we use a temperature profile that ensures that the locally isothermal temperature distribution is valid close to either star. The circumprimary and circumsecondary disc temperatures should be dominated by the primary and secondary star irradiation, respectively. We adopt the sound speed distribution (proportional to the square root of the temperature) of Farris et al. (2014) and set the sound speed c_s to be

$$c_s = c_{s0} \left(\frac{a}{M_1 + M_2} \right)^q \left(\frac{M_1}{R_1} + \frac{M_2}{R_2} \right)^q , \quad (4)$$

where $R_i = |\boldsymbol{R} - \boldsymbol{R}_i|$ with i = 1, 2 are the radial distances from the primary and the secondary star, respectively, and c_{s0} is a constant of proportionality. The sound speed given by equation (4) ensures that close to primary (secondary) the temperature of the disc is set by the primary (secondary), while for $R_i \gg a$ the sound speed is set by the distance from the centre of mass of the binary. Furthermore, the distribution ensures a smooth transition for material that moves from one star to the other. For $q = 0$, the sound speed is constant and the disc is globally isothermal. For a disc of vertical scale height H with $q = 0.5$, the disc aspect ratio H/R_i is constant in radius close to either star, $R_i \ll a$. With the exception of the simulations in Section 3.1, we take $q = 0.75$. We consider an initial configuration with a highly misaligned accretion disc around only one component of a circular equal mass binary. The binary has total mass $M = M_1 + M_2 = 1$ and a circular orbit in the x–y plane with separation a. We choose the accretion radius for the particle removal to be $R_{acc} = 0.025\,a$ around each component of the binary. The mass and angular momentum of any particle that enters the sink radius are added to that of the sink particle.

The circumprimary disc initially has a mass of $M_d = 0.001\,M$, and it is inclined with respect to the binary orbital plane. The initial surface density profile is set as $\Sigma \propto (R_1/R_{in})^{-3/2}(1 - \sqrt{R_{in}/R_1})$ between $R_{in} = 0.025\,a$ and $R_{out} = 0.25\,a$.

With this density distribution and a sound speed distribution given by equation (4) for $q = 0.75$, the disc is uniformly resolved. The circumsecondary disc is taken to be initially absent, i.e. its density distribution is initially zero. Tides from the companion star can overcome the viscous torque and truncate the disc (Paczynski 1977; Papaloizou & Pringle 1977; Goldreich & Tremaine 1980; Artymowicz & Lubow 1994). These torques transfer angular momentum from the disc to the orbit of the binary. The outer radius is chosen to be the tidal truncation radius for the disc assuming a coplanar binary. Since misaligned discs feel a weaker torque compared to coplanar discs, the outer edge of the disc might be larger than this value (Lubow, Martin & Nixon 2015; Miranda & Lai 2015; Nixon & Lubow 2015). We vary the other parameters: disc aspect ratio, viscosity, initial inclination, and binary mass ratio (see Table 1).

In the simulations, we identify particles as belonging to the circumprimary, circumsecondary, and circumbinary discs at a given time. To do this, we calculate the specific energy of each particle

Table 1. Parameters of the circumprimary disc for each simulation. The first column contains the label for each simulation, the second column is the slope of the circumprimary disc temperature profile, the third column contains the disc aspect ratio at the inner edge, the fourth column is the binary mass ratio, the fifth and sixth columns contain the disc viscosity and initial inclination, respectively. Column 7 shows the binary eccentricity, and column 8 shows the circumprimary disc outer radius is units of the binary separation. Column 9 shows the amount of mass accreted on to the secondary star after a time of 40 P_b, $\Delta M/M_d$. The last column contains the respective figures in the paper for each simulation.

ID	q	$H/R_1(R_{in})$	M_2/M_1	α	i	e_b	R_{out}/a	$\Delta M/M_d$	Fig.
run1	0	0.01	1.0	0.1	60°	0	0.25	0.018	3
run2	0.5	0.03	1.0	0.1	60°	0	0.25	0.038	3, 4
run3	0.75	0.01	1.0	0.1	60°	0	0.25	0.0078	5
run4	0.75	0.035	1.0	0.1	60°	0	0.25	0.029	5, 6, 7, 8
run5	0.75	0.035	1.0	0.01	60°	0	0.25	0.0065	7
run6	0.75	0.035	0.5	0.1	60°	0	0.25	0.042	8, 9
run7	0.75	0.05	1.0	0.1	70°	0	0.25	0.11	10,11, 12
run8	0.75	0.035	1.0	0.1	70°	0	0.25	0.055	–
run9	0.75	0.05	1.0	0.1	70°	0.5	0.2	0.03	13

to see whether it is bound to the central object within the Roche lobe it occupies. To determine which particles belong to the circumbinary disc (see Section 4), we require that the particles orbit around the binary and are energetically bound to it. Since both the circumprimary and the newly formed circumsecondary disc respond in a global fashion when subjected to KL oscillations in these simulations, we consider as representative values the averages of both the eccentricity and inclination over the whole disc radial extent.

3.1 Disc formation and effects of the temperature distribution

We show that mass transfer can occur from the primary disc to form a secondary disc. We also explore the effects of the disc temperature profile on the mass transfer process. We compare the results of the simulations with the same viscosity coefficient $\alpha = 0.1$ and an equal mass binary, but using different equations of state. The sound speed profiles are described by equation (4). We apply a globally isothermal profile ($q = 0$, run1) and a spatially varying temperature profile with $q = 0.5$ (run2). The different q values change the temperature structure, which in turn change the disc aspect ratios about each star i, H/R_i , where H is the disc scale height. The globally isothermal equation of state implies the disc aspect ratio increases with radius, while equation (4) implies a constant disc aspect ratio for $q = 0.5$. For comparison, we choose circumprimary discs that have the same aspect ratio at radius $R_1 = R_{out}$. We compare a globally isothermal disc with $H/R_1\,(R_{out}) = 0.03$ with a locally isothermal disc ($q = 0.5$) with constant $H/R_1 = 0.03$ (i.e. we compare run1 with run2). In these cases, the disc aspect ratios at the initial inner edges are $H/R_1\,(R_{in}) = 0.01$ and 0.03 for the $q = 0$ and $q = 0.5$ cases, respectively.

The bottom panel of Fig. 3 plots the total amount of mass accreted into the sink about the secondary (within a distance of $R_{acc} = 0.025a$ of the secondary) in units of the initial circumprimary disc mass, $\Delta M/M_d$, as a function of time in units of the binary orbital period. The amount of mass accreted on to the secondary star is about a factor of 2 higher in the locally isothermal $q = 0.5$ case. This increase is due to the fact that the amplitude of the KL oscillations of the disc eccentricity is larger in the constant disc aspect ratio case ($q = 0.5$) than in the globally isothermal case ($q = 0$).

The four upper panels of Fig. 3 show the eccentricity and inclination evolution of the circumprimary (left-hand panels) and circumsecondary (right-hand panels) discs. In both cases, the circumsecondary disc forms with non-zero initial eccentricity and

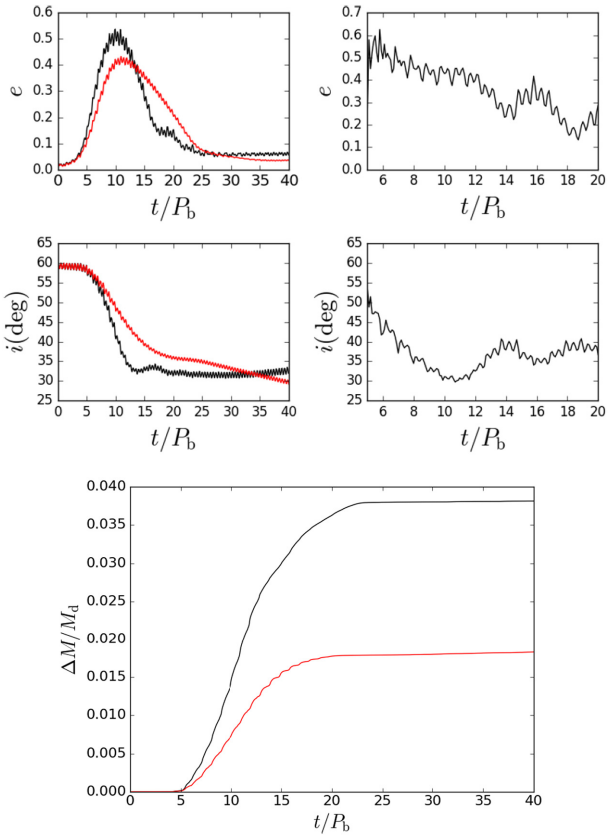

Figure 3. Top four panels: Eccentricity (upper panels) and inclination (lower panels) evolution of the circumprimary (left) and circumsecondary (right) disc averaged over the whole disc. Bottom panel: Accreted mass within a distance of $R_{acc} = 0.025\,a$ from the secondary star scaled by the initial circumprimary disc mass $\Delta M/M_d$ as a function of time in units of P_b. The black lines refer to the disc sounds speed described in equation (4) with $q = 0.5$ (run2), while the red lines are for a globally isothermal simulation ($q = 0$, run1).

inclination above the critical KL angle i_{cr} for an initially circular test particle orbit. We show the eccentricity and inclination of the circumsecondary disc only for the $q = 0.5$ locally isothermal simulation because of the lack of resolution for the circumsecondary disc in the globally isothermal case. In the $q = 0.5$ simulation (the

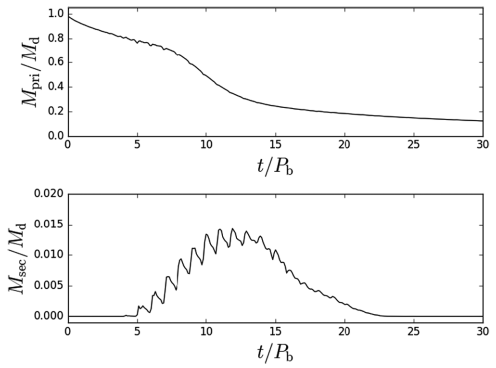

Figure 4. Mass contained in the circumprimary (upper panel) and circumsecondary (lower panel) discs outside $R_{\rm acc} = 0.025\,a$ from the central star in units of the initial circumprimary disc mass $M_{\rm d} = 0.001$M as a function of time in units of $P_{\rm b}$. The disc sounds speed is described in equation (4) with $q = 0.5$ (run2).

black line), we see that the circumsecondary disc undergoes a KL oscillation.

The KL oscillation period of the circumsecondary disc in the $q = 0.5$ case is shorter than the circumprimary disc oscillation period, in agreement with the test particle calculations presented in Section 2. The minimum tilt angle of the circumsecondary disc is significantly below the critical angle $i_{\rm cr} \simeq 39^\circ$ for initially circular test particle orbits. Minimum tilt angles below $i_{\rm cr}$ can be produced for test particles that start with a non-zero eccentricity, as discussed in Section 2. But since the circumprimary disc inclination also reaches below $i_{\rm cr}$, other effects such as disc dissipation or gas pressure may play a role.

Fig. 4 plots the amount of mass contained in the circumprimary (upper panel) and circumsecondary (lower panel) discs in units of the initial circumprimary disc mass $M_{\rm d} = 0.001$M as a function of time for the simulation with sound speed given by equation (4) with $q = 0.5$ (run2). Notice that, while the lowest panel of Fig. 3 plots $\Delta M/M_{\rm d}$, the amount of mass accreted within a distance $R_{\rm acc}$ from the secondary star, Fig. 4 plots the amount of mass within each Roche lobe outside distance $R_{\rm acc}$ that is also energetically bound to each star. The circumsecondary disc starts with zero mass and it acquires mass as the first KL oscillation begins. After roughly 22 $P_{\rm b}$, the circumsecondary disc has been almost completely accreted on to the secondary star.

In the remainder of this work, we use the Farris et al. (2014) sound speed distribution given by equation (4) with $q = 0.75$ to describe the temperature profile of the circumprimary disc and to model the circumsecondary disc formed as a consequence of the transfer of mass through Roche lobe overflow.

3.2 Effects of the circumprimary disc aspect ratio

The amount of mass transferred to the secondary star depends crucially on the value of the disc aspect ratio of the circumprimary disc. The main effects that play a role are essentially two: the disc has to spread fast enough in order for its outer edge to fill the Roche lobe and at the same time the material in the circumprimary disc cannot be drained too quickly through accretion on to the primary star. The disc aspect ratio affects both processes. A lower (higher) value of H/R_1 corresponds to slower (faster) viscous spreading, while also leading to a lower (higher) accretion rate on to the primary star.

High disc sound speeds can suppress KL oscillations. Zanazzi & Lai (2017) and Lubow & Ogilvie (2017) showed that the critical

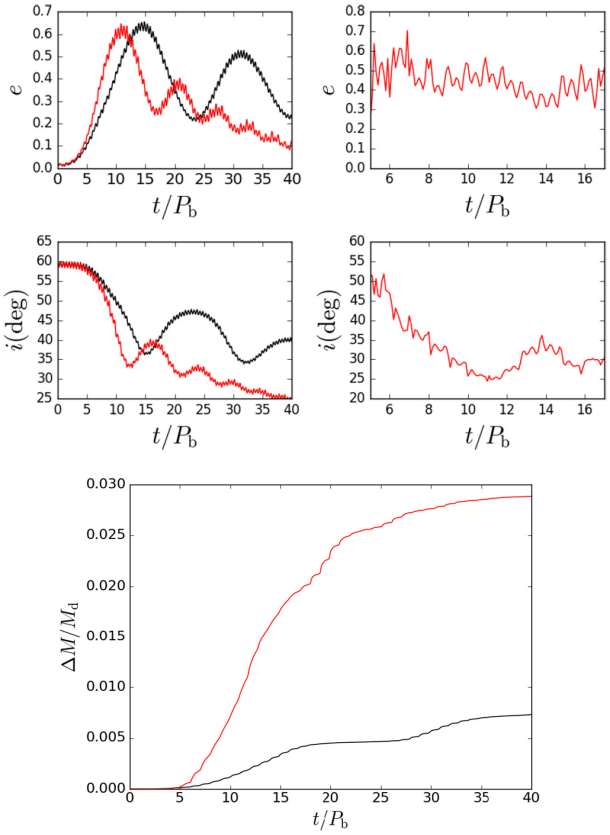

Figure 5. Top four panels: Eccentricity (upper panels) and inclination (lower panels) evolution of the circumprimary (left) and circumsecondary (right) disc averaged over the whole disc. Bottom panel: Accreted mass within $R_{\rm acc} = 0.025\,a$ of the secondary star scaled by the initial circumprimary disc mass $\Delta M/M_{\rm d}$ as a function of time in units of $P_{\rm b}$. The black curves refer to a circumprimary aspect ratio $H/R_1(R_{\rm in}) = 0.01$ (run3), while the red lines are for $H/R_1(R_{\rm in}) = 0.035$ (run4). The sound speed varies in radius according to equation (4) with $q = 0.75$.

inclination angle for KL oscillations to occur changes with the disc aspect ratio. According to fig. 2 of Lubow & Ogilvie (2017), if the disc aspect ratio $H/R \gtrsim 0.15$ at the disc outer edge in an equal mass binary, then there are typically no KL modes present, due to the effects of pressure on the disc apsidal precession. Thus, the disc would not undergo KL oscillations and there would be no mass transfer between the components of the binary.

Fig. 5 shows the effect of changing the disc aspect ratio with other parameters held constant in simulations and $q = 0.75$ in equation (4). We consider disc aspect ratios at the disc inner edge $H/R_1(R_{\rm in}) = 0.01$ (run3) and $H/R_1(R_{\rm in}) = 0.035$ (run4), represented by the black and red curve, respectively. The top panels show the eccentricity (upper panel) and the inclination (lower panel) of the primary (left) and secondary (right) discs. The smaller disc aspect ratio (the black curves) leads to higher amplitude KL oscillations in the primary disc. The oscillations are slightly delayed and have a longer period. This delay may explain in part the smaller amount of mass being transferred to the secondary star during the 40 $P_{\rm b}$ of the simulation. In both cases, the disc aspect ratios H/R_1 at the disc inner edges are small enough to prevent fast accretion on to the primary star. In addition, the disc aspect ratios at the disc outer edges are also small enough to prevent fast outward spreading of the disc. The higher $H/R_1 = 0.035$ case results in faster outward spreading than

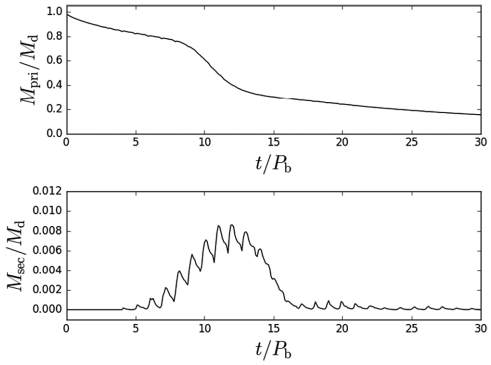

Figure 6. Mass contained in the circumprimary (upper panel) and circumsecondary (lower panel) discs outside $R_{\rm acc}$ of the central stars in units of the initial circumprimary disc mass $M_{\rm d} = 0.001$M as a function of time in units of $P_{\rm b}$. The disc sound speed is described in equation (4) with $q = 0.75$ and $H/R_1(R_{\rm in}) = 0.035$ (run4).

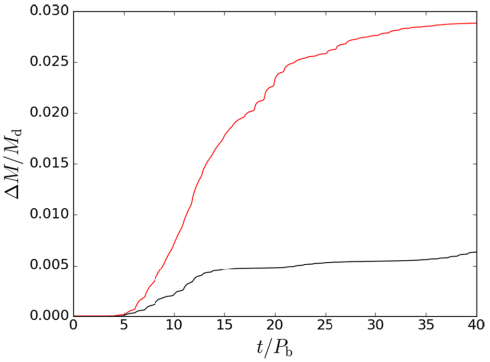

Figure 7. Accreted mass within a radius $R_{\rm acc}$ of the secondary star scaled by the initial circumprimary disc mass $\Delta M/M_{\rm d}$ as a function of time in units of $P_{\rm b}$. The black line refers to $\alpha = 0.01$ (run5), while the red line refers to $\alpha = 0.1$ (run4). The sound speed varies in radius according to equation (4) with $q = 0.75$.

in the lower $H/R_1 = 0.01$, which may also explain the higher mass accretion rate on to the secondary for the higher H/R_1 case.

As seen in Figs 5 and 6, the transfer of mass between the two binary components is triggered after roughly 5 $P_{\rm b}$, when the circumprimary disc eccentricity begins to grow. In the upper left-hand panels of Fig. 5, we show the eccentricity and inclination of the circumsecondary disc only for the higher aspect ratio simulation (run4). Again, we see evidence for tilt oscillations with circumsecondary disc periods that are shorter than circumprimary disc periods, as discussed in Section 3.1. For the lower aspect ratio simulation (run3), there are not enough particles around the secondary to properly resolve the accretion disc behaviour and so we do not plot the corresponding results for that case.

As a test of the importance of KL oscillations to the mass transfer process, we ran a model with an initial tilt that is too low for KL oscillations to occur. We compare the amount of mass accreted on to the secondary star in the higher aspect ratio simulation (run4) that has an initial disc inclination of 60° to that obtained with the same parameters, but with the initial circumprimary disc inclination of 40°. In this case, the disc does not undergo KL oscillations and the amount of mass accreted on to the companion is negligibly small ($\Delta M/M_{\rm d} \sim 10^{-5}$ after 40 $P_{\rm b}$). Therefore, it is clear that the mass transfer mechanism is KL oscillations.

3.3 Disc viscosity

The disc viscosity provides the source of angular momentum transport causing the disc to spread outwards on the viscous time-scale $t_\nu = R^2/\nu$. According to the α-prescription (Shakura & Sunyaev 1973), for a fixed gas–temperature distribution a lower value of α implies slower disc spreading. Fig. 7 shows the amount of accreted mass within radius $R_{\rm acc}$ of the secondary normalized by the initial circumprimary disc mass $\Delta M/M_{\rm d}$ as a function of time, in units of the binary period, for two different values of the viscosity parameter $\alpha = 0.01$ and 0.1 (i.e. we compare run4 and run5), represented by the black and red curves, respectively. Decreasing the viscosity by an order of magnitude results in a decrease in the amount of mass accreted on to the secondary by roughly a factor of 3. With a smaller viscosity, the circumprimary disc spreads out more slowly. Since the time-scale for the period of the KL oscillations decreases with distance from the primary, the smaller primary disc has a longer KL oscillation period. Furthermore, the smaller disc leads to less mass transfer to the secondary. However, the mass transfer on to the secondary star is not suppressed, but is delayed in time. A smaller viscosity value leads also to slower accretion on to the primary star. Therefore, there would be more material in the circumprimary disc that can eventually be transferred to the secondary star.

Note that the values of the viscosity parameter used in this work, $\alpha = 0.01$ and 0.1, are large compared to the value inferred from the observations of protoplanetary discs, i.e. $10^{-4}-10^{-3}$ (e.g. Pinte et al. 2016; Flaherty et al. 2017). As we discussed in the introduction, the inability to model such low-viscosity values with SPH codes is a limitation. However, the dynamical effect of viscosity depends on the kinematic viscosity ν that depends on the disc aspect ratio, as well as α. While we cannot set α to a very small value, we can lower the disc aspect ratio to obtain the same correspondent kinematic viscosity. For instance, in the simulation run5 we obtain the same kinematic viscosity of a typical protostellar disc with $H/R = 0.1$ and $\alpha \sim 10^{-4}$.

3.4 Binary mass ratio

We consider the effects of changing the binary mass ratio on the mass transfer process. In the bottom panel of Fig. 8, we compare the accreted mass on to the secondary star for two different values of the mass ratio $\mu = 0.5$ and 1.0 (i.e. we compare run6 and run4). The figure shows that the amount of mass transferred to the secondary increases for the small mass ratio case. This effect may be due to the weaker torque exerted by a less massive companion that acts to prevent gas from entering its Roche lobe. But other effects may play a role, such as the properties of the KL oscillations.

The upper four panels of Fig. 8 show the eccentricity and inclination of the circumprimary (left-hand panels) and circumsecondary (right-hand panels) disc evolution with time. A smaller mass ratio leads to an increased time-scale for the KL oscillations. The disc is eccentric for longer so it can transfer more mass on to the secondary star (see bottom panel in Fig. 8). We plot the eccentricity and inclination evolution of the circumsecondary disc of the simulation with $\mu = 0.5$ (run6), which is to be compared with the equal mass binary simulation (run4) in Fig. 5.

As also seen in the upper panels of Fig. 8, the effect of decreasing the mass ratio of the binary components $\mu = M_2/M_1$ is essentially to cause a delay in the KL oscillations and therefore a delay in the mass transfer, as was also found by Fu et al. (2015a).

In the simulations, this delay may be explained by the fact that the initial disc around the primary has to spread farther out for the

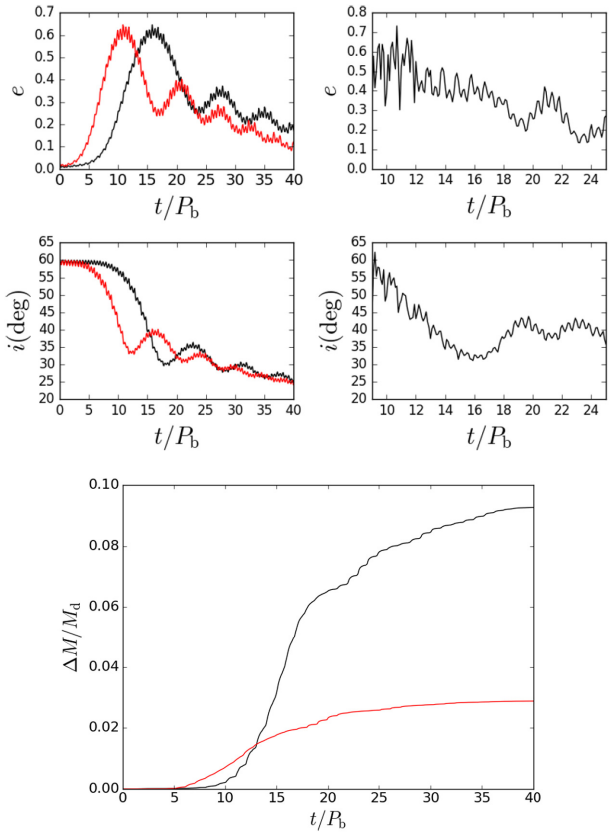

Figure 8. Top four panels: Eccentricity (upper panels) and inclination (lower panels) evolution of the circumprimary (left) and circumsecondary (right) disc as a function of time in units of P_b averaged over the whole disc. Bottom panel: Accreted mass within a distance of $R_{acc} = 0.025\,a$ from the secondary star scaled by the initial circumprimary disc mass $\Delta M/M_d$ as a function of time in units of P_b. The black and red lines refer to mass ratios 0.5 (run6) and 1.0 (run4), respectively. The sound speed varies in radius according to equation (4) with $q = 0.75$.

torque exerted by the secondary to be strong enough to trigger KL oscillations.

Furthermore, we see a hint of KL oscillations of the circumsecondary disc in the simulation with binary mass ratio $\mu = 0.5$ at around 20 P_b. This has a period of about 5 P_b, which is roughly half the KL oscillation period of the (initially circular) circumprimary disc. Fig. 9 shows the amount of mass contained in the circumprimary (upper panel) and circumsecondary (lower panel) disc in units of the initial circumprimary disc mass $M_d = 0.001$M as a function of time for the simulation with lower binary mass ratio (run6).

3.5 Circumprimary disc initial misalignment angle

We investigate the effect of the initial inclination angle of the circumprimary accretion disc on the amount of mass that is transferred to the secondary star and how it affects the circumsecondary disc formation. Using the similar model parameters to run4 in Table 1 and a higher disc aspect ratio $H/R_1(R_{in}) = 0.05$, we increase the initial inclination of the disc around the primary to $i = 70°$ for run7.

We first compare the amount of mass transferred for different simulations with the same aspect ratio and different circumprimary disc initial inclination to isolate the effect of the latter. We found that a higher inclination leads to an increase of the mass transferred by

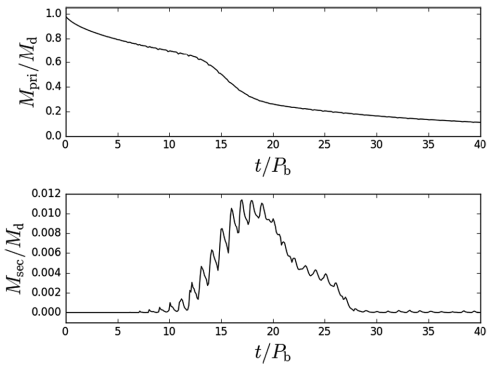

Figure 9. Mass contained in the circumprimary (upper panel) and circumsecondary (lower panel) discs outside R_{acc} of the central stars in units of the initial circumprimary disc mass $M_d = 0.001$M as a function of time in units of P_b for the simulation in run6.

roughly a factor 2 (comparison between run7 and run8 in Table 1). Since we now know that a higher disc aspect ratio at the inner edge leads to higher mass transfer, we ran the same simulation with a higher value of $H/R_1(R_{in})$ to better resolve the circumsecondary disc.

We define a Cartesian coordinate system whose origin is at the binary centre of mass and corotates with the binary. The x-axis is along the direction from the centre of mass to the secondary star. The z-axis is along the direction of the binary angular momentum. The results of the SPH simulation run7 are shown in Fig. 10. The surface density of the accretion discs is shown in the $x-y$, $x-z$, and $y-z$ planes for times of $t = 0$, 5, 10, and 20 P_b.

Fig. 10 shows how the disc formation process operates. The KL oscillations of the circumprimary disc result in an increase of its eccentricity from its initially circular form. The apastron distance increases in the outer disc to be large enough for some material to enter into the Roche lobe of the companion. It can clearly be seen that the material is transferred from the primary to the secondary. The flow occurs in the form of a gas stream. The stream of material that flows into the secondary Roche lobe has angular momentum about the secondary and therefore does not directly impact it. This material is on an eccentric orbit around the secondary. The stream of material self-intersects and dissipates energy via shocks. Both discs can be seen to be highly eccentric and misaligned at $t = 10$ P_b. At a time $t = 20$ P_b, only the secondary disc contains enough mass to be visible on the plot. Since the circumprimary disc is inclined with respect to the binary orbit, the material enters the Roche lobe of the secondary with a non-zero inclination and therefore the resulting accretion disc is misaligned to the binary orbital plane. The bottom panels of Figs 11 and 12 show that there is more mass transferred to the secondary than in the previous cases that have an initial inclination of 60°. As seen in the upper left-hand panel, increasing the initial disc inclination leads to more accretion within the accretion radius of the primary star because the disc becomes more eccentric during the KL oscillations (see equation 3). The circumprimary disc is completely accreted after roughly 20 P_b, which corresponds to two KL oscillations of its eccentricity and inclination. However, the amplitude of the oscillations is larger. Thus, the mass transfer to the secondary is more efficient. As seen in the upper right-hand panel of Fig. 11, the circumsecondary disc starts forming after 5 P_b when the first KL oscillation occurs. The amount of mass transferred to the secondary star after 40 P_b is $\Delta M/M_d = 0.11$.

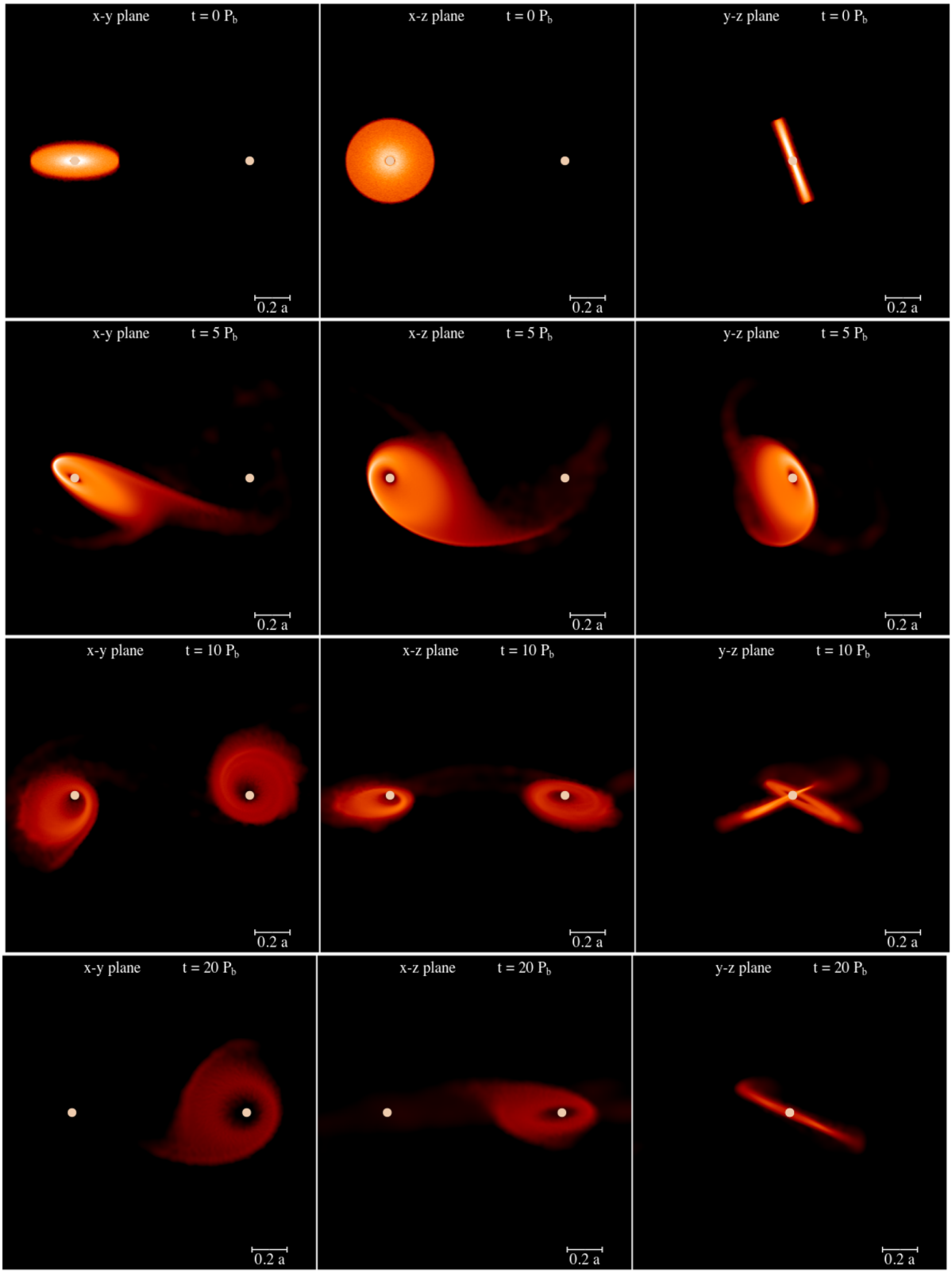

Figure 10. SPH simulation of a binary (shown by the white circles) with a disc around the primary star forming a circumsecondary disc through KL oscillations. The system is plotted in the frame that is corotating with the binary. The size of the circles denotes the accretion radius of the SPH sink particle. The panels show the view looking down the $x-y$, $x-z$, and $y-z$ planes. The binary orbit lies in the $x-y$ plane. The circumprimary is initially tilted from the binary orbital plane by 70° and becomes eccentric due to the KL mechanism. The parameters are the fiducial ones with sound speed defined by equation (4) and $H/R_1(R_{\rm in}) = 0.05$. The panels refer to times $t = 0$, 5, 10, and 20 $P_{\rm b}$ (from top to bottom row). Only one star is shown in the right-hand panels because the stars lie on top of each other.

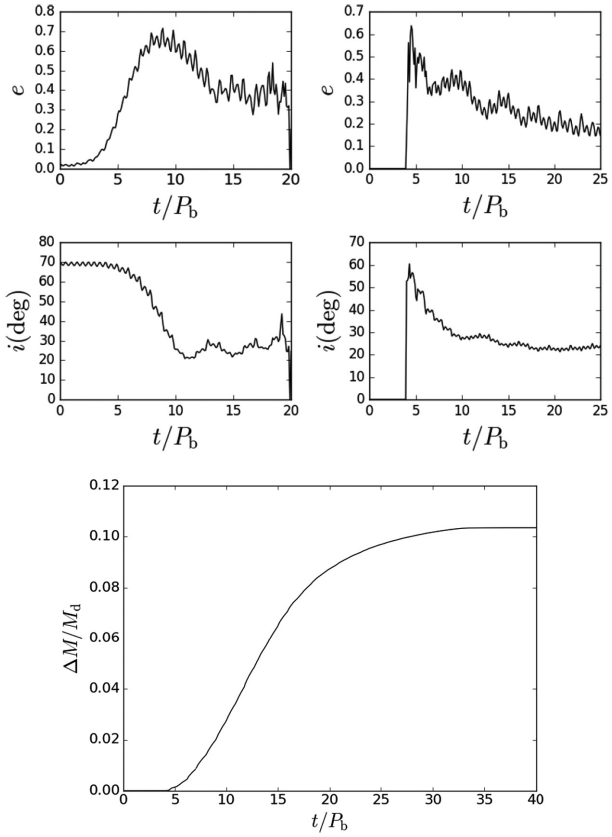

Figure 11. Top four panels: Eccentricity (upper panels) and inclination (lower panels) evolution of the circumprimary (left) and circumsecondary (right) disc as a function of time in units of P_b averaged over the whole disc for a disc with an initial inclination of 70° (run7). Bottom panel: Accreted mass within a distance of $R_{acc} = 0.025\,a$ from the secondary star scaled by the initial circumprimary disc mass $\Delta M/M_d$ as a function of time in units of P_b.

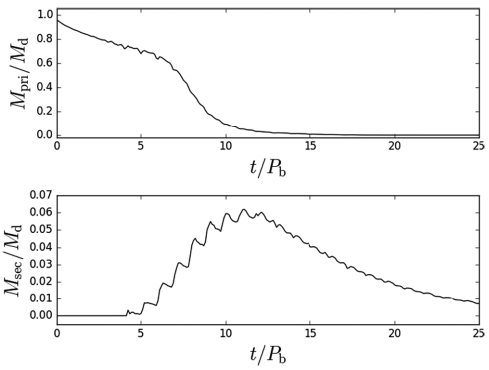

Figure 12. Mass contained in the circumprimary (upper panel) and circumsecondary (lower panel) discs outside R_{acc} of the central stars in units of the initial circumprimary disc mass $M_d = 0.001$M as a function of time in units of P_b for the simulation in run7.

The comparison between the upper four left-hand and right-hand panels of Fig. 11 shows that an initially eccentric accretion disc experiences KL oscillations on a shorter period compared to the circular case, as discussed in Section 3.1.

Fig. 12 shows the amount of mass contained in the circumprimary (upper panel) and circumsecondary (lower panel) disc in units of the initial circumprimary disc mass $M_d = 0.001$M as a function of time. The circumsecondary disc starts with zero mass and it acquires mass as the first KL oscillation begins. The circumsecondary disc contains more mass than the circumprimary disc at times later than $\sim$12 P_b. After roughly 25 P_b, the circumsecondary disc has been largely accreted on to the secondary star.

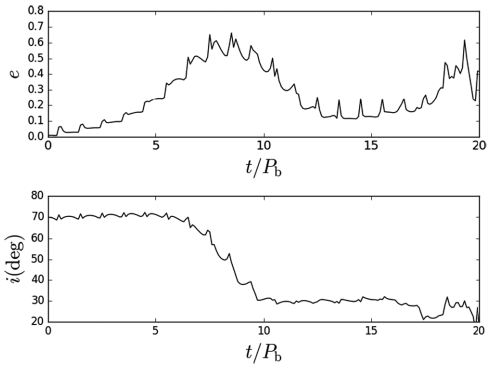

Figure 13. Eccentricity (upper panel) and inclination (lower panel) evolution of the circumprimary disc as a function of time in units of P_b averaged over the whole disc for a disc with an initial inclination of 70°, disc outer radius $R_{out} = 0.2a$, and binary eccentricity $e_b = 0.5$ (run9).

3.6 Binary eccentricity

The observed binary orbital eccentricities vary with binary orbital period (Raghavan et al. 2010; Tokovinin & Kiyaeva 2016). The closest binaries with periods less than 10 days are circularized by tidal dissipation. The average binary eccentricity increases as a function of binary orbital period and ranges from about 0.4 to 0.6. We investigate the effect of the binary eccentricity on the mass transfer from the circumprimary disc by running a simulation (run9) with the same parameters as run7 of Section 3.5 that involves a circular orbit binary, except that we take the binary eccentricity to be $e_b = 0.5$. We also reduced the circumprimary disc outer radius to $R_{out} = 0.2\ a$ since the torque exerted by the eccentric binary is stronger and this results in a smaller truncation radius (Artymowicz & Lubow 1994; Fu et al. 2015a).

Fig. 13 shows the circumprimary disc eccentricity and inclination evolution as a function of time in units of the binary orbital period. After 20 P_b the circumprimary disc is accreted. The amount of mass transferred to the secondary star, roughly 3 %, is much lower than we find for a circular binary in run7, 11 %. We do not show the evolution of the newly formed circumsecondary disc, since we do not have enough resolution to see KL oscillations. However, as in the circular case, the circumsecondary disc forms with non-zero eccentricity ($e \approx 0.6$) and at a high inclination ($i \approx 60°$). So it is likely that this disc is subject to KL oscillations.

4 CIRCUMBINARY DISC FORMATION

As the circumprimary disc undergoes KL oscillations of eccentricity, some of the material that escapes the Roche lobe of the primary is captured in orbit around the binary. The same process might also occur though overflow of a pre-existing circumsecondary disc, if it were included in the simulations. The material self-intersects and circularizes forming a circumbinary disc. Fig. 14 shows the surface density profile of the circumsecondary and circumbinary disc after 24 P_b. This profile is the result of the simulation described

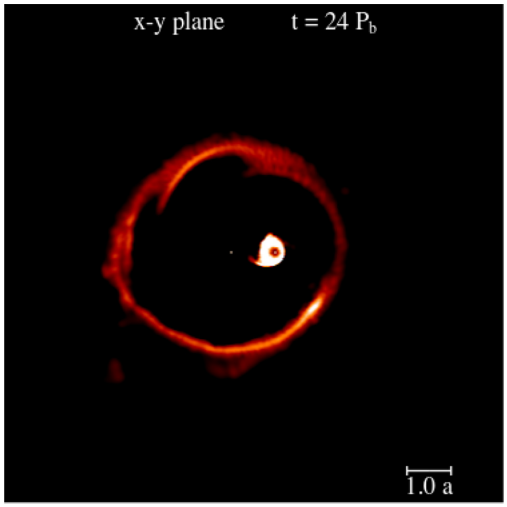

Figure 14. SPH simulation of a binary (shown by the red circles) with a disc around the primary star forming a circumsecondary and a circumbinary disc through KL oscillations (run7). The size of the red circles denotes the accretion radius of the SPH sink particles. The surface density is plotted in the $x-y$ plane after 24 P_b.

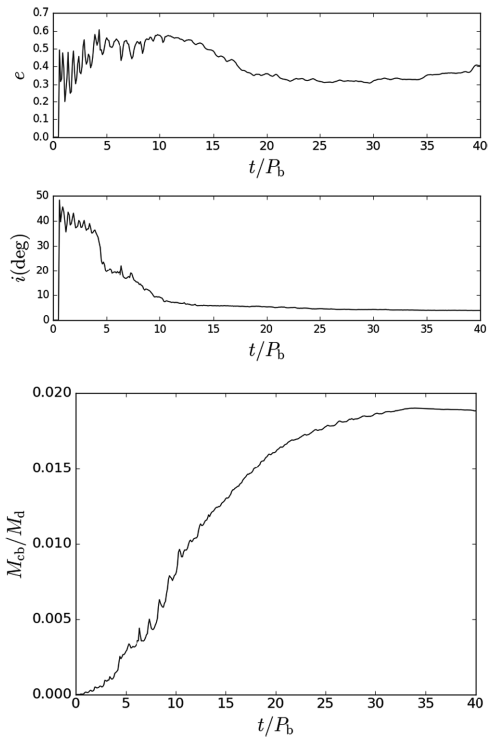

Figure 15. Upper and middle panel: Eccentricity and inclination evolution of the circumbinary disc. Bottom panel: Amount of mass contained in the circumbinary disc as a function of time, in units of the initial circumprimary disc mass. The parameters of the circumprimary disc are $\alpha = 0.1$, and $H/R(R_{in}) = 0.05$, initial disc tilt $i = 70^\circ$, and the binary is equal mass (run7).

in Section 3.5. The newly formed circumbinary disc extends from $R_{in} \sim a$ up to roughly $R_{out} \sim 5a$. The eccentricity and inclination of the circumbinary disc are shown in Fig. 15, where we average the quantities over the whole disc.

In the simulation, we identify particles as belonging to the circumbinary disc if they lie outside the binary and are energetically bound to the binary. The circumbinary disc that forms is highly eccentric and mildly inclined with respect to the binary plane. The eccentricity decreases slightly with time, while the disc gradually aligns with the binary plane over 40 P_b. The amount of mass that remains in the circumbinary disc at the end of the simulation is around 1–2 % of the initial circumprimary disc mass if the binary is circular. The lower panel of Fig. 15 shows the mass of the circumbinary disc, in units of the circumprimary disc initial mass, as a function of time in units of the binary orbit.

A problem related to planet formation in circumbinary accretion discs in tight binaries is that the discs have been found to be rather compact and might be not massive enough to form giant planets (Harris et al. 2012). We found the newly formed circumbinary disc to be radially very narrow in our simulations. The viscous evolution of a compact disc is faster compared to one of an extended disc. Therefore, accretion of this disc material on to the binary occurs on a shorter time-scale, and this could significantly reduce the available time in which planets could form. Furthermore, circumbinary discs formed in this way contain only 1 % of the initial circumprimary disc mass, and this could be another obstacle for planet formation. However, it is likely that the material that forms the circumbinary disc in our simulation will add to an already present circumbinary disc. Thus, the mechanism described here increases the amount of circumbinary material. If the binary has an eccentricity of $e_b = 0.5$ (run9), almost 10 % of the initial circumprimary disc mass is captured by the binary. Therefore, there is more material that can add to an already present disc than in the circular binary case.

The newly formed circumbinary disc is likely to spread initially, but would eventually be accreted on to the binary, as is known for coplanar circumbinary discs (Artymowicz & Lubow 1996). Furthermore, since this disc forms eccentric and inclined with respect to the orbital plane of the binary, its interaction with an already present disc might lead to a change in its eccentricity and inclination.

5 CONCLUSIONS

We analysed the evolution of an initially misaligned disc around the primary star in a circular and eccentric orbit binary system with no initial circumsecondary disc. We have found that when the circumprimary disc undergoes KL oscillations of eccentricity and inclination, it transfers mass to the secondary that results in the formation of a misaligned circumsecondary disc. The circumsecondary disc also undergoes KL oscillations. The two discs are misaligned with respect to each other as well as with respect to the binary orbital plane. In addition, some circumprimary gas flows outwards to form a circumbinary disc.

The amount of mass that is transferred from the primary to the secondary star through KL oscillations depends on several parameters of both the circumprimary disc and the binary itself. Within the range of parameters we examine, increasing the disc aspect ratio, its viscosity, and initial inclination angle leads to larger amount of mass transfer on to the secondary. It is generally of order of $\lesssim 10\%$ of the initial primary disc mass. Decreasing the binary mass ratio also leads to a larger amount of mass transfer. However, we expect that the behaviour changes at more extreme values of some of these parameters. For example, at sufficiently high viscosity and small secondary mass, the accretion on to the primary will occur before a KL disc oscillation is well underway. Also, the KL disc mechanism is suppressed at higher disc sound speeds (Lubow & Ogilvie 2017; Zanazzi & Lai 2017). In such cases, KL mass transfer mechanism will not operate. Binary eccentricity

appears to decrease the amount of gas captured by the secondary and increase the amount of gas in the circumbinary disc. Further analysis of the effects of binary eccentricity would be worth pursuing.

The SPH simulations performed in this work are scale free. Therefore, the results could in principle be applied to both wide and close binaries. The typical size of observed circumstellar discs is up to a few hundred au. Therefore, in the case of HK Tau, with binary separation ∼350 au, the KL oscillation mechanism may be operating. However, if the binary separation is large compared to the disc size it might be difficult for the circumprimary disc to fill the Roche lobe of the primary star and to create a misaligned disc around the companion star within the lifetime of the primary disc.

It is likely that both components of a binary star system form with an accretion disc, and these discs may be misaligned to each other and to the binary orbital plane. In a more complete model, there will be mass transfer between the two components. The material transferred to each component will change the angular momentum and eccentricity of a disc that already exists. In a future publication, we will investigate the interaction of the accreted material with an already present circumsecondary disc.

ACKNOWLEDGEMENTS

We thank Mario Livio for useful discussions. We thank Daniel Price for providing the PHANTOM code for SPH simulations and acknowledge the use of SPLASH (Price 2007) for the rendering of the figures. We acknowledge support from NASA through grant NNX17AB96G. Computer support was provided by UNLV's National Supercomputing Center.

REFERENCES

Artymowicz P., Lubow S. H., 1994, ApJ, 421, 651
Artymowicz P., Lubow S. H., 1996, ApJ, 467, L77
Bate M. R., 2009, MNRAS, 392, 590
Bate M. R., 2012, MNRAS, 419, 3115
Bate M. R., 2018, MNRAS, 475, 5618
Bate M. R., Bonnell I. A., Price N. M., 1995, MNRAS, 277, 362
Bate M. R., Lodato G., Pringle J. E., 2010, MNRAS, 401, 1505
Batygin K., 2012, Nature, 491, 418
Doğan S., Nixon C., King A., Price D. J., 2015, MNRAS, 449, 1251
Fabrycky D., Tremaine S., 2007, ApJ, 669, 1298
Farris B. D., Duffell P., MacFadyen A. I., Haiman Z., 2014, ApJ, 783, 134
Flaherty K. M. et al., 2017, ApJ, 843, 150
Ford E. B., Rasio F. A., 2008, ApJ, 686, 621
Fu W., Lubow S. H., Martin R. G., 2015a, ApJ, 807, 75
Fu W., Lubow S. H., Martin R. G., 2015b, ApJ, 813, 105
Fu W., Lubow S. H., Martin R. G., 2017, ApJ, 835, L29
Goldreich P., Tremaine S., 1980, ApJ, 241, 425
Harris R. J., Andrews S. M., Wilner D. J., Kraus A. L., 2012, ApJ, 751, 115
Horch E. P., Howell S. B., Everett M. E., Ciardi D. R., 2014, ApJ, 795, 60
Innanen K. A., Zheng J. Q., Mikkola S., Valtonen M. J., 1997, AJ, 113, 1915
Jensen E. L. N., Akeson R., 2014, Nature, 511, 567
Jensen E. L. N., Mathieu R. D., Donar A. X., Dullighan A., 2004, ApJ, 600, 789
King A. R., Livio M., Lubow S. H., Pringle J. E., 2013, MNRAS, 431, 2655
Kozai Y., 1962, AJ, 67, 591
Kratter K., Lodato G., 2016, ARA&A, 54, 271
Lidov M. L., 1962, Planet. Space Sci., 9, 719
Lodato G., Price D. J., 2010, MNRAS, 405, 1212
Lodato G., Pringle J. E., 2007, MNRAS, 381, 1287
Lubow S. H., Martin R. G., 2016, ApJ, 817, 30
Lubow S. H., Ogilvie G. I., 2017, MNRAS, 469, 4292
Lubow S. H., Martin R. G., Nixon C., 2015, ApJ, 800, 96
Martin R. G., Nixon C., Lubow S. H., Armitage P. J., Price D. J., Doğan S., King A., 2014, ApJ, 792, L33
Martin R. G., Lubow S. H., Nixon C., Armitage P. J., 2016, MNRAS, 458, 4345
Meru F., Bate M. R., 2012, MNRAS, 427, 2022
Miranda R., Lai D., 2015, MNRAS, 452, 2396
Moutou C. et al., 2009, A&A, 498, L5
Nixon C., Lubow S. H., 2015, MNRAS, 448, 3472
Nixon C., King A., Price D., 2013, MNRAS, 434, 1946
Nixon C. J., 2012, MNRAS, 423, 2597
O'Toole S. et al., 2009, ApJ, 697, 1263
Offner S. S. R., Kratter K. M., Matzner C. D., Krumholz M. R., Klein R. I., 2010, ApJ, 725, 1485
Paczynski B., 1977, ApJ, 216, 822
Papaloizou J., Pringle J. E., 1977, MNRAS, 181, 441
Pinte C., Dent W. R. F., Ménard F., Hales A., Hill T., Cortes P., deGregorio-Monsalvo I., 2016, ApJ, 816, 25
Price D. J. et al., 2017, Astrophysics Source Code Library, record ascl:1709.002
Price D. J., 2007, Publ. Astron. Soc. aust., 24, 159
Price D. J., 2012, J. Comput. Phys., 231, 759
Price D. J., Federrath C., 2010, MNRAS, 406, 1659
Raghavan D. et al., 2010, ApJS, 190, 1
Roccatagliata V., Ratzka T., Henning T., Wolf S., Leinert C., Bouwman J., 2011, A&A, 534, A33
Shakura N. I., Sunyaev R. A., 1973, A&A, 24, 337
Stapelfeldt K. R., Krist J. E., Ménard F., Bouvier J., Padgett D. L., Burrows C. J., 1998, ApJ, 502, L65
Tamuz O. et al., 2008, A&A, 480, L33
Tokovinin A., Kiyaeva O., 2016, MNRAS, 456, 2070
Wu Y., Murray N., 2003, ApJ, 589, 605
Xiang-Gruess M., Papaloizou J. C. B., 2013, MNRAS, 431, 1320
Zanazzi J. J., Lai D., 2017, MNRAS, 467, 1957

This paper has been typeset from a TEX/LATEX file prepared by the author.